Heating and cooling of protons by turbulence-driven ion cyclotron waves in the fast solar wind

Xing Li and Shadia R. Habbal
Harvard-Smithsonian Center for Astrophysics, Cambridge, Massachusetts

Joseph V. Hollweg
Institute for the Study of Earth, Oceans and Space and Department of Physics, University of New Hampshire, Durham, New Hampshire

Ruth Esser
Harvard-Smithsonian Center for Astrophysics, Cambridge, Massachusetts

Abstract

The effects of parallel propagating nondispersive ion cyclotron waves on the solar wind plasma are investigated in an attempt to reproduce the observed proton temperature anisotropy, namely, $T_{p\perp} >> T_{p\|}$ in the inner corona and $T_{p\perp} < T_{p\|}$ at 1 AU. Low-frequency Alfvén waves are assumed to carry most of the energy needed to accelerate and heat the fast solar wind. The model calculations presented here assume that nonlinear cascade processes, at the Kolmogorov and Kraichnan dissipation rates, transport energy from low-frequency Alfvén waves to the ion cyclotron resonant range. The energy is then picked up by the plasma through the resonant cyclotron interaction. While the resonant interaction determines how the heat is distributed between the parallel and perpendicular degrees of freedom, the level of turbulence determines the net dissipation. Ion cyclotron waves are found to produce a significant temperature anisotropy starting in the inner corona, and to limit the growth of the temperature anisotropy in interplanetary space. In addition, this mechanism heats or cools protons in the direction parallel to the magnetic field. While cooling in the parallel direction is dominant, heating in the parallel direction occurs when $T_{p\perp} >> T_{p\|}$. The waves provide the mechanism for the extraction of energy from the parallel direction to feed into the perpendicular direction. In our models, both Kolmogorov and Kraichnan dissipation rates yield $T_{p\perp} >> T_{p\|}$ in the corona, in agreement with inferences from recent ultraviolet coronal measurements, and predict temperatures at 1 AU which match in situ observations. The models also reproduce the inferred rapid acceleration of the fast solar wind in the inner corona and flow speeds and particle fluxes measured at 1 AU. Since this mechanism does not provide direct energy to the electrons, and the electron-proton coupling is not sufficient to heat the electrons to temperatures at or above 10^6 K, this model yields electron temperatures which are much cooler than those currently inferred from observations.

1. Introduction

Recent measurements of the inner corona by the Ultraviolet Coronagraph Spectrometer (UVCS) [*Kohl et al.*, 1995] on board SOHO have provided the first evidence for the existence of a temperature anisotropy of protons and heavy ions in polar coronal holes within 5 R_s of the solar surface. Measurements of the resonantly scattered Lyman α spectral line, from which information on the protons is derived [see *Allen et al.*, 1998], and of spectral lines from other heavy ions, such as O^{+5}, have shown that the spread of their velocity distribution in the direction perpendicular to the magnetic field, or effective temperature, $T_\perp$, is much larger than that in the parallel direction, or $T_\|$ [*Kohl et al.*, 1998; *Li et al.,* 1998]. For protons, the inferred ratio $T_{p\perp}/T_{p\|}$ reaches a maximum of about 4 below 5 R_s. Earlier in situ Helios observations of the fast solar wind in the ecliptic plane yielded an average ratio of 1.7 at 0.3 AU, decreasing to 0.8 at 1 AU [*Marsch et al.*, 1982a].

Clearly, the development of a temperature anisotropy in the inner corona and its persistence into interplanetary space have important implications for the mechanisms responsible for coronal heating and solar wind acceleration. Attempts to include the proton temperature anisotropy in solar wind models were made earlier by *Leer and Axford* [1972] and more recently by *Sandbæk and Leer* [1994] and *Hu et al.* [1997]. In these studies an ad hoc heating function was used. While the *Leer and Axford* [1972] and *Sandbæk and Leer* [1994] studies reproduced conditions typical of the slow solar wind, the work by *Hu et al.* [1997] tried to match the characteristics of the fast solar wind. One of the original results of the *Hu et al.* [1997] study was the finding that the inclusion of a proton temperature anisotropy in the models requires that either the protons be highly anisotropic in the inner corona or that a mechanism, in addition to adiabatic expansion, must exist to cool protons in the direction parallel to the magnetic field. *Hu et al.* [1997] also noted that the heating due to Alfvén wave dissipation was not sufficient to account for the observed proton temperature at 1 AU.

Numerical simulations of magnetized plasmas showed that ion cyclotron waves not only heat ions in the direction perpendicular to the magnetic field but, interestingly enough, also cool them in the parallel direction when the wave frequency is lower than the ion cyclotron frequency [*Busnardo-Neto et al.*, 1976]. *Arunasalam* [1976] proved that indeed this phenomenon could be accounted for by the quasi-linear theory of ion-cyclotron-resonant interaction in the resonant limit. The process basically involves the transfer of energy from the parallel to the perpendicular motions when the energy in the waves is below the energy available at the ion cyclotron resonance frequency.

Since low-frequency Alfvén waves are commonly observed in the solar wind [*Smith et al.*, 1995; *Belcher and Davis*, 1971] and are the low-frequency manifestation of ion cyclotron waves, they provide an attractive mechanism for the development of the temperature anistropy. Power spectra of magnetic field fluctuations in the solar wind, most likely of Alfvénic nature, are typically of the form $P_B \propto k^{-\eta}$, where k is the wavenumber and η the spectral index. Since observations yield $1.4 \leq \eta \leq 2.0$ [*Behannon*, 1978; *Bavassano et al.*, 1982], most of the power in the Alfvénic fluctuations is in the frequency range below the ion cyclotron frequency. Hence no substantial influence of these waves on ions can be expected [see *Isenberg and Hollweg*, 1983; *Marsch et al.,* 1982b]. This difficulty can be overcome if the Sun launches waves in the ion cyclotron resonance range leading to the heating and acceleration of the solar wind [e.g., *Tu and Marsch,* 1995; *Axford and McKenzie*, 1995; *McKenzie et al.*, 1995, 1997; *Tu and Marsch*, 1997], or if there exists some mechanism which replenishes the resonant wave power as soon as it is absorbed by the particles.

To tap into the energy available in Alfvénic fluctuations, *Hollweg* [1986] assumed that a nonlinear cascade process, namely, the Kolmogorov dissipation of Alfvénic turbulence, transports energy from the low-frequency waves to the ion cyclotron resonant range, where it is picked up by the plasma through the resonant cyclotron interaction. *Hollweg and Johnson* [1988] extended this idea to a two-fluid solar wind model. Their results yielded the right qualitative features: a steep temperature rise in the transition region to over 10^6 K in the corona and acceleration to supersonic speeds. However, they noted that their model predicted coronal proton temperatures which were higher than those suggested by the data available at that time. Following that approach, *Isenberg* [1990] used the Kolmogorov dissipation rate in a three fluid solar wind model starting at 1.5 R_s. The dissipated energy was distributed to protons and alpha particles according to the resonant cyclotron interaction of these species with a spectrum of parallel-propagating ion cyclotron waves. *Isenberg* [1990] again dismissed this dissipation rate because it produced a much higher proton temperature in the inner corona than the observed values then available, and yielded proton temperatures about a factor of 2 lower than measured at 1 AU.

The goal of this paper is to show that the cascading and dissipation mechanism first proposed by *Holl-*

weg [1986] can account for the observed temperature anisotropy of protons in the inner corona as well as in interplanetary space. The impetus for this study is provided by (1) the recent inferences of proton temperatures and anisotropies in the fast solar wind by *Kohl et al.* [1996, 1998], which are in the range predicted by the models of *Hollweg and Johnson* [1988] and *Isenberg* [1990]; (2) the potential need for a cooling mechanism for protons in the parallel direction as indicated by *Hu et al.* [1997]; and (3) the recent observations by *Leamon et al.* [1998], who note that a spectral break and steepening of the power spectrum at the high-frequency end suggests the onset of dissipation there.

Unlike the approaches by *Hollweg and Johnson* [1988] and *Isenberg* [1990], our study includes proton thermal conduction and proton temperature anisotropy as described in section 2. Although proton thermal conduction observed at 1 AU is about 2 orders of magnitude smaller than the classical value [e.g., *Esser et al.,* 1997], it is shown in section 3 that proton thermal conduction could possibly limit the proton temperature in the inner corona. This study explores the Kraichnan dissipation rate (section 3.5) in addition to the Kolmogorov rate (sections 3.2–3.4 and 3.6). We also show how the latitudinal dependence of the proton temperature anisotropy, governed by the Parker spiral field and the stability of the solar wind solutions, depends on the strength of the interplanetary magnetic field (section 3.7). We conclude in section 4 with a discussion of the limitations of this approach.

2. Model Description

2.1. A Two-Fluid Model With Anisotropic T_p

Following the approach by *Hu et al.* [1997], the one-dimensional time-dependent equations governing the electron-proton solar wind flow with anisotropic proton temperature, in the presence of Alfvén waves, can be written in the following form:

$$\frac{\partial n}{\partial t} + \frac{1}{a}\frac{\partial}{\partial r}(nva) = 0, \tag{1}$$

$$\begin{aligned}\frac{\partial v}{\partial t} + v\frac{\partial v}{\partial r} + \frac{k_B}{m_p}\left(\frac{\partial T_{p\parallel}}{\partial r}\cos^2\Phi + \frac{\partial T_{p\perp}}{\partial r}\sin^2\Phi + \frac{\partial T_e}{\partial r}\right) \\ + \frac{k_B}{nm_p}\left(T_{p\parallel}\cos^2\Phi + T_{p\perp}\sin^2\Phi + T_e\right)\frac{\partial n}{\partial r} \\ + \frac{k_B}{am_p}\left(T_{p\parallel} - T_{p\perp}\right)\frac{\partial}{\partial r}\left(a\cos^2\Phi\right) + \frac{GM_s}{r^2} \\ - \frac{k_B}{2m_p a}\frac{da}{dr}\left(T_{p\parallel} - T_{p\perp}\right)\sin^2\Phi - \frac{1}{nm_p}F_w = 0,\end{aligned} \tag{2}$$

$$\begin{aligned}\frac{\partial T_e}{\partial t} + v\frac{\partial T_e}{\partial r} + \frac{(\gamma-1)T_e}{a}\frac{\partial}{\partial r}(va) \\ - \frac{\gamma-1}{nk_B a}\frac{\partial}{\partial r}\left(\kappa_e a\cos^2\Phi\frac{\partial T_e}{\partial r}\right) + 2\nu_{pe}\left(T_e - T_p\right) \\ - \frac{\gamma-1}{nk_B}(Q_e - L_{\rm rad}) = 0,\end{aligned} \tag{3}$$

$$\begin{aligned}\frac{\partial T_{p\parallel}}{\partial t} + v\frac{\partial T_{p\parallel}}{\partial r} + 3(\gamma-1)T_{p\parallel}\cos^2\Phi\frac{\partial v}{\partial r} \\ + \frac{3(\gamma-1)}{2a}\frac{\mathrm{d}a}{\mathrm{d}r}vT_{p\parallel}\sin^2\Phi + \frac{3(\gamma-1)}{nk_B a}\frac{\partial}{\partial r}\left(aq_{p\parallel}\right) \\ + 2\nu_{pe}\left(T_{p\parallel} - T_e\right) + 2\nu_{pp}\left(T_{p\parallel} - T_{p\perp}\right) - \frac{3(\gamma-1)}{nk_B}Q_{p\parallel} = 0,\end{aligned} \tag{4}$$

$$\begin{aligned}\frac{\partial T_{p\perp}}{\partial t} + v\frac{\partial T_{p\perp}}{\partial r} + \frac{3(\gamma-1)}{2}T_{p\perp}\sin^2\Phi\frac{\partial v}{\partial r} \\ - \frac{3(\gamma-1)}{4a}\frac{\mathrm{d}a}{\mathrm{d}r}vT_{p\perp}\sin^2\Phi + \frac{3(\gamma-1)}{2nk_B a}\frac{\partial}{\partial r}\left(aq_{p\perp}\right) \\ + \frac{3(\gamma-1)vT_{p\perp}}{2a}\frac{\mathrm{d}a}{\mathrm{d}r} + 2\nu_{pe}\left(T_{p\perp} - T_e\right) \\ - \nu_{pp}\left(T_{p\parallel} - T_{p\perp}\right) - \frac{3(\gamma-1)}{2nk_B}Q_{p\perp} = 0.\end{aligned} \tag{5}$$

Neutrality and zero current are assumed so that $n_e \approx n_p = n$, and $v_e \approx v_p = v$ is assumed to be radial. The solar mass and gravitational constant are M_s and G, respectively, while $\gamma = 5/3$ is the adiabatic index, k_B is the Boltzmann constant, and m_p is the proton mass. The electron temperature is T_e. The electron heating term, Q_e, in equation (3), is introduced in the models as an ad hoc heating function of the form [e.g., *Withbroe*, 1988]

$$Q_e = Q_{e0} n_e e^{(R_s - r)/\sigma_e}, \tag{6}$$

when the thermal coupling between electrons and protons is not sufficient to drive the solar wind. Here Q_{e0}, σ_e are adjustable constants, and R_s is the solar radius. The function $L_{\rm rad}$ describing the radiative energy loss in the electron energy equation (3) is assumed to have the form parameterized by *Rosner et al.* [1978] for an optically thin medium. The mean proton temperature is defined as $T_p = (T_{p\parallel} + 2T_{p\perp})/3$, where $T_{p\parallel}$ and $T_{p\perp}$ are the proton temperature parallel and perpendicular to the magnetic field, respectively. The proton heating terms in the direction parallel, $Q_{p\parallel}$, and perpendicular, $Q_{p\perp}$, to the magnetic field direction, as well as the force due to the Alfvén waves, F_w, are described in section 2.2.

The angle between the magnetic field and the radial direction, Φ, is given by [*Hollweg and Johnson*, 1988; *Hu et al.*, 1997]

$$\tan\Phi = \begin{cases} (\Omega r/v)\sin\theta & r > 10\ R_s, \\ 0 & r \le 10\ R_s. \end{cases} \tag{7}$$

Here $\Omega = 2.7\times10^{-6}$ radian s^{-1} is the angular velocity of the Sun, and θ is the heliospheric colatitude, varying from 0° at the pole to 90° at the equator. Unless otherwise stated, the results shown are for $\theta = 90°$ to illustrate the effect of the spiral field, and for comparison with the ecliptic in situ measurements of temperature anisotropies, which are the only ones currently available.

The collision frequencies ν_{pe} and ν_{pp} are [*Hu et al.*, 1997]

$$\nu_{pe} = \frac{4\sqrt{2\pi m_e}\, ne^4 \ln\Lambda}{3 m_p k_B^{3/2} T_e^{3/2}} \,,\; \nu_{pp} = \frac{4\sqrt{\pi}\, ne^4 \ln\Lambda}{3\sqrt{m_p} k_B^{3/2} T_p^{3/2}} \,, \quad (8)$$

where ln Λ is the Coulomb logarithm. The heat conductive flux densities $q_{p\parallel}$ and $q_{p\perp}$, corresponding to the transport of energy along the interplanetary magnetic field associated with the parallel and perpendicular thermal motions of the protons, are given by [*Sandbæk and Leer*, 1994]

$$q_{p\parallel} = -\frac{1}{3}\kappa_p \cos^2\Phi\; T_p^{5/2}\, \frac{\partial T_{p\parallel}}{\partial r}, \quad (9)$$

$$q_{p\perp} = -\frac{2}{3}\kappa_p \cos^2\Phi\; T_p^{5/2}\, \frac{\partial T_{p\perp}}{\partial r}. \quad (10)$$

When $T_{p\parallel}$ is equal to $T_{p\perp}$, adding (9) and (10) yields the heat flux density for an isotropic proton gas. In order to reproduce the small proton thermal conduction observed in interplanetary space, we adopt the following expressions for the thermal conduction coefficient [*Hu et al.*, 1997]:

$$\frac{\kappa_p}{\kappa_{pc}} = \begin{cases} 1 & R_s < r \le r_1, \\ (r_2 - r + \varepsilon_p \frac{(r-r_1)}{(r_2-r_1)} & r_1 < r \le r_2, \\ \varepsilon_p & r > r_2, \end{cases} \quad (11)$$

where r_1, r_2 and ε_p are adjusted in the computations to give values of q_p which agree with those derived from in situ observations at 1 AU. The classical expressions for the coefficients κ_{ec} and κ_{pc} for ln $\Lambda = 23$ are given by [*Spitzer*, 1962; *Braginskii*, 1965]

$$\kappa_e = \kappa_{ec} = 8\times10^{-7}\, T_e^{5/2},\; \kappa_{pc} = 3.2\times10^{-8}\, T_p^{5/2}. \quad (12)$$

2.2. Evolution of Alfvén Waves

In the presence of a temperature anisotropy, the dispersion relation of outward propagating nondispersive waves in the cold plasma approximation can be written as [*Barnes and Suffolk*, 1971]

$$\omega/k_\parallel = v_\parallel + A^{1/2}\, v_A \quad (13)$$

with

$$A = \left[1 + \frac{4\pi(p_\perp - p_\parallel)}{B^2 + \langle\delta B^2\rangle}\right] \,, \quad (14)$$

where $v_A = B/\sqrt{4\pi\rho_p}$ is the Alfvén speed, $p_\perp$ and $p_\parallel$ are the proton pressures in the direction perpendicular and parallel to the magnetic field, $\left\langle\delta B^2\right\rangle^{1/2}$ is the magnetic field fluctuation in the Alfvén waves, and B is the average local magnetic field strength. As can be seen from equation (14), $A = 1$ for an isotropic fluid. In a spherically symmetric flow, when the Alfvén waves damp, the wave force F_w on the protons can be written as [*Isenberg and Hollweg*, 1982]

$$F_w = \rho_p \frac{\mathrm{d}}{\mathrm{d}r}\left[\frac{4\pi p_w}{B^2}(\omega^2/k_\parallel^2 - v_\parallel^2)\right] + \frac{Q_p v_\parallel}{(\omega/k_\parallel - v_\parallel)v}, \quad (15)$$

where Q_p is the proton heating rate due to the dissipation of Alfvén waves. Using the wave equations given by *Isenberg* [1984], the wave force F_w can then be rewritten as

$$F_w = -\frac{1}{8\pi A}\frac{\mathrm{d}[A^2\langle\delta B^2\rangle]}{\mathrm{d}r}. \quad (16)$$

This result was given by *Barnes* [1979] for dissipationless waves. (In the appendix, we show that it also holds for dissipative waves.)

The time-dependent wave energy equation can be written as [*Isenberg*, 1984]

$$\frac{\partial}{\partial t}[(1+A)p_w] + \nabla\cdot\mathbf{F} + vF_w + Q_p = 0, \quad (17)$$

where

$$\mathbf{F} = 8\pi p_w \left[\frac{\rho_p v_\parallel(\omega/k_\parallel - v_\parallel)^2}{2B^2} + \frac{(p_\perp - p_\parallel)\omega}{(B^2 + 8\pi p_w)k_\parallel} + \frac{\omega}{4\pi k_\parallel}\right]\mathbf{B}/B. \quad (18)$$

is the wave energy flux and

$$p_w = \frac{\langle\delta B^2\rangle}{8\pi} \quad (19)$$

is the magnetic pressure exerted by Alfvén waves when $A = 1$. The velocity fluctuations $\langle\delta v^2\rangle$ of Alfvén waves in an anisotropic fluid are then given by

$$\langle\delta v^2\rangle = \frac{A\langle\delta B^2\rangle}{4\pi\rho_p} = \frac{2Ap_w}{\rho_p}. \quad (20)$$

The total heating rate, Q_p, is distributed to protons in the parallel, $Q_{p\parallel}$, and perpendicular, $Q_{p\perp}$, directions according to the quasi-linear theory of the ion cyclotron resonant interaction of particles with a wave power spectrum $P_B(k_\parallel) \propto k_\parallel^{-\eta}$ [see *Arunasalam*, 1976; *Dusenbery and Hollweg*, 1981; *Marsch et al.*, 1982b; *Isenberg*, 1984]. In the following we assume that the proton distribution function can be approximated by a bi-Maxwellian. The parallel and perpendicular heating of the protons from the waves can then be written as

$$Q_{p\parallel} = Q_p \frac{Q^w_{p\parallel}}{Q^w_{p\parallel} + Q^w_{p\perp}}, \; Q_{p\perp} = Q_p \frac{Q^w_{p\perp}}{Q^w_{p\parallel} + Q^w_{p\perp}}, \quad (21)$$

with [see *Isenberg*, 1984]

$$Q^w_{p\perp} = \rho_p \frac{q_p^2}{m_p^2} \left(\frac{m_p}{T_{p\parallel}}\right)^{1/2} \int_0^\infty dk_\parallel \; k_\parallel^{-(\eta+1)} \frac{\Omega_p}{k_\parallel} H_p \quad (22)$$

$$Q^w_{p\parallel} = \rho_p \frac{q_p^2}{m_p^2} \left(\frac{m_p}{T_{p\parallel}}\right)^{1/2} \cdot \int_0^\infty dk_\parallel k_\parallel^{-(\eta+1)} \left(\frac{\omega - \Omega_p}{k_\parallel} - v_\parallel\right) H_p \quad (23)$$

where

$$H_p = \{\Omega_p/k_\parallel + [(\omega - \Omega_p)/k_\parallel - v_\parallel]/\Gamma_p\} \cdot \exp\{-m_p(2k_B T_{p\parallel})^{-1}[(\omega - \Omega_p)/k_\parallel - v_\parallel]^2\}, \quad (24)$$

where ω and $k_\parallel$ are the wave frequency and wave number, respectively. The cyclotron frequency of the protons is $\Omega_p = q_p B/m_p$, q_p is the proton charge, Γ_p is the anisotropy $T_{p\parallel}/T_{p\perp}$, and $v_\parallel$ is the solar wind speed in the frame corotating with the Sun. We note that while the integration is from 0 to ∞, the dominant contribution to the integral occurs in the vicinity of the inverse of the local ion inertial length, i.e., in the vicinity of $k_\parallel \approx \Omega_p/v_A$.

2.3. Computational Approach

A fully implicit time-dependent, one-dimensional, two-fluid solar wind code is used to solve equations (1) to (5) and (17). Details of the computational scheme are given by *Hu et al.* [1997]. There are 1000 non uniformly distributed grid points used to cover the distance from 1 to 258 R_s. The smallest grid distance is about $10^{-6} R_s$ at the coronal base, which guarantees a very good accuracy where gradients are steepest. The maximum error in any of the conserved quantities is less than 1% once a steady state is reached.

Boundary conditions at the coronal base, $r = 1\ R_s$, are such that the density, temperature of all species and Alfvén wave velocity amplitude, $\langle\delta v^2\rangle^{1/2}$, are kept fixed there, while the velocity of the protons/electrons is determined by the mass conservation equation with $\partial n/\partial t = 0$. Linear extrapolation is used for all quantities at the outer boundary.

3. Numerical Results

3.1. Heating Rates and Input Parameters

Model computations with proton heating at the Kolmogorov and Kraichnan dissipation rates are presented here. The heating of the protons at the Kolmogorov rate is given by [*Hollweg*, 1986]

$$Q_p = \Gamma \rho_p \langle\delta v^2\rangle^{3/2}/L_c, \quad (25)$$

while the Kraichnan heating rate is written as [*Hollweg and Johnson,* 1988]

$$Q_p = \Gamma \rho_p \langle\delta v^2\rangle^2/(L_c v_A). \quad (26)$$

Here L_c is the correlation length of the fluctuations, Γ is a dimensionless parameter, and ρ_p is the proton mass density.

Following *Hollweg* [1986], the correlation length is chosen to scale as the distance between flow tubes

$$L_c \propto \sqrt{a}, \quad (27)$$

where $a = r^2 f(r)$ is the cross section of a flow tube with

$$f(r) = \frac{f_m e^{(r-r_a)/\sigma_a} + 1 - (f_m - 1)e^{(R_s - r_a)/\sigma_a}}{e^{(r-r_a)/\sigma_a} + 1}, \quad (28)$$

taken from *Kopp and Holzer* [1976]. Here f_m, r_a, and σ_a are adjustable constants which determine how rapidly, and where, most of the expansion of the field lines occurs.

For all models, the density and temperature at the coronal base are fixed at

$$n_e = 2.5 \times 10^8 \mathrm{cm}^{-3}, \quad T_e = T_{p\parallel} = T_{p\perp} = 6 \times 10^5 \mathrm{K}. \quad (29)$$

The corresponding base pressure $n_e T_e$ is consistent with values given by *Withbroe* [1977, 1988] and *Dulk et al.* [1977] in coronal holes. The magnetic field at the coronal base is computed from the conservation of magnetic flux for a given value B_{rE} at 1 AU, and a cross-section a, i.e.,

$$B = 215^2\ B_{rE}\ f_m \ \ \mathrm{G} \quad (30)$$

with B_{rE} in units of 10^{-5} G (or γ). In the examples that follow, $B_{rE} = 5\gamma$ unless otherwise specified.

In addition, the following choice of adjustable parameters is made and is kept the same for all models unless otherwise indicated:

$$\varepsilon_p = 0.02, r_1 = 3\ R_s,\ r_2 = 8\ R_s, \quad \left(\langle\delta v^2\rangle^{1/2}\right)_{1_{R_s}} = 25\ \mathrm{km/s} \quad (31)$$

$\left(\langle\delta v^2\rangle^{1/2}\right)_{1_{R_s}}$ is always chosen below the upper limit of 35 km/s currently inferred from remote sensing observations [e.g., *Esser et al.*, 1998b and references therein].

In all model computations, the choice of parameters is such as to achieve the same wind speed and mass flux at 1 AU, except for model 2, as will be described next.

3.2. Dissipation at the Kolmogorov Rate With $\eta = 5/3$

We consider first the Kolmogorov rate with a spectral slope $\eta = 5/3$ and a purely radial geometry with $f_m = 1$ (model 1). In this example there is no additional heating to electrons, and the correlation length is

$$(L_c/\Gamma)_{1_{R_s}} = 9 \times 10^4 \text{ km}. \qquad (32)$$

The corresponding solar wind parameters are shown in Figure 1 together with the empirical values currently available from remote sensing observations of the inner corona. The velocity (Figure 1a), electron density (Figure 1b), and temperatures (Figure 1c), match as closely as possible the empirical constraints on electron density in the inner corona [from *Fisher and Guhathakurta*, 1995], perpendicular and parallel components of proton temperature [from *Kohl et al*, 1998], and flow speeds and temperature components in interplanetary space [*Marsch et al.,* 1989]. For comparison with observations of line widths derived from UVCS measurements, the effective temperature T_{eff}, given by

Figure 1

$$T_{\text{eff}} = T_{p\perp} + \frac{m_p}{2k}\langle \delta v^2 \rangle, \qquad (33)$$

is also shown (as a dashed line) in Figure 1c. The anisotropy, given by $T_{p\parallel}/T_{p\perp}$, and the ratio $\langle \delta B^2 \rangle^{1/2}/B$ are displayed in Figure 1d as solid and dotted lines, respectively. This model yields the following parameters at 1 AU:

$$\begin{array}{l} v_E = 748 \text{ km/s}, \; n_E = 2.95 \text{ cm}^{-3}, \\ T_p = (2T_{p\perp} + T_{p\parallel})/3 = 3.88 \times 10^5 \text{ K}, \\ T_e = 3.8 \times 10^4 \text{ K}, \; \langle \delta B^2 \rangle^{1/2}/B = 0.52, \end{array} \qquad (34)$$

which, with the exception of electrons, are in very good agreement with observations. The wind velocity of 270 km s^{-1} at 4 R_s is at the lower limit of the recent UVCS observations [*Kohl et al.,* 1998]. The gradual acceleration is similar to that of all wave-driven models [e.g., *Esser et al.*, 1987]. The ratio $\langle \delta B^2 \rangle^{1/2}/B$ is within the limits of 0.5-0.96 derived from Helios measurements at 1 AU [*Villante and Vellante,* 1982; *Roberts,* 1989], and 0.5 from Ulysses measurements at high latitudes [*Balogh et al.*, 1995; *Smith et al.,* 1995]. Electrons have a maximum temperature of 7×10^5 K at 1.3 R_s, which is significantly lower than the peak value of about $T_e = 1.5 \times 10^6$ K inferred from a number of measurements [e.g., *Habbal et al.*, 1993; *Esser et al.*, 1998a], and too low compared with in situ values beyond 60 R_s [e.g., *Schwenn,* 1990].

The proton temperature anisotropy develops quickly after 1.5 R_s and decreases to a minimum value of $T_{p\parallel}/T_{p\perp} = 0.2$ around 8 R_s. This is consistent with inferences from UVCS observations [*Kohl et al.,* 1998]. The proton anisotropy $T_{p\parallel}/T_{p\perp}$ at 1 AU is comparable to the observed value of 1.2 ± 0.45 [*Marsch et al.,* 1982a]. The proton parallel temperature beyond 100 R_s decreases more rapidly than in the models of *Hu et al.* [1997]. The cooling of the protons stems from the adiabatic expansion of the solar wind plasma, including radial expansion associated with $\partial v/\partial r$, and transverse expansion associated with da/dr, the latter being larger than the former in general. The transverse expansion affects the parallel cooling when the magnetic field deviates from the radial direction by a finite angle Φ (see equation (4)). Nevertheless, Φ is small within 1 AU for high-speed streams; it is less than 30° at 1 AU in the equatorial plane and much smaller still at high latitudes, in fact zero at the poles. Therefore the effect of transverse expansion on parallel cooling is essentially negligible within 1 AU for the fast wind. The radial expansion can cause parallel cooling, but it depends on $\partial v/\partial r$ (see equation (4)) and thus is important only near the Sun. Beyond 100 R_s, the acceleration of the wind has already been achieved, and the parallel cooling of the protons by the radial expansion is completely negligible. Based on similar arguments, *Hu et al.* [1997] concluded that a parallel cooling mechanism is needed in the high-speed stream beyond about 50 R_s if that temperature component is high in the inner corona.

In fact, as described by equations (22)-(24), and studied in detail by *Dusenbery and Hollweg* [1981] and *Busnardo-Neto et al.* [1976], the cooling occurs primarily when the wave frequency is smaller than the cyclotron frequency. The effect of the ion cyclotron resonance can also be followed from the changes in the heating rates $Q_{p\perp}$ and $Q_{p\parallel}$ as a function of heliocentric distance, as shown in Figure 1e. The solid lines correspond to positive values, while the dashed lines correspond to negative values. We note that $Q_{p\perp}$ is always positive; hence protons always get heated in the perpendicular direction. But $Q_{p\parallel}$ is very different. Protons get cooled at the coronal base and beyond 50 R_s, when $Q_{p\parallel} < 0$. However, between 1.5 and 50 R_s, protons are also heated in the parallel direction. According to (23), $Q_{p\parallel}$ can be positive when $T_{p\parallel} << T_{p\perp}$. At 1 AU, $Q_{p\parallel}$ has the same order of magnitude as $Q_{p\perp}$. Since $Q_p = Q_{p\parallel} + Q_{p\perp}$, is fixed by equation (25) at a given heliocentric distance, the negative $Q_{p\|}$ leads to a larger heating in the perpendicular direction. The thermal energy of protons in the parallel direction has thus been transferred to the perpendicular direction. Hence ion cyclotron waves not only produce a strong proton temperature anisotropy in the inner corona but also limit the growth of the proton temperature anisotropy in interplanetary space.

For comparison, the parallel cooling term in (4)

$$-\frac{nk_B}{2a}\frac{\mathrm{d}a}{\mathrm{d}r}vT_{p\|}\sin^2\Phi$$

which is due to the spiral magnetic field, is shown as a dotted line in Figure 1e. We note that the parallel cooling of protons from ion cyclotron waves is as important as that from the spiral magnetic field between 60 R_s and 1 AU except in polar regions where magnetic field lines are radial and the cooling due to ion cyclotron waves is dominant.

Finally, we compare the wave force and the proton pressure gradient force, i.e., all terms involving $T_{p\|}$ and $T_{p\perp}$ in equation (2). These are shown in Figure 1f. While the wave force is always smaller than the proton pressure gradient force, its effect increases very rapidly from the coronal base reaching a maximum around 10 R_s, then decreases very gradually out to 1 AU. Hence, even though Alfvén waves supply all the energy needed to accelerate and heat the solar wind, the wave force does not play a dominant role in the acceleration process. This is why wave-driven solar wind models do not yield a very steep velocity gradient in the inner corona. The acceleration is completed via the energy transfer from the waves to the thermal energy of the plasma. At 1 AU the net kinetic and potential energies gained between 1 R_s and 1 AU are 0.96 and 0.67 erg cm^{-2} s^{-1} respectively, while the energy flux lost from Alfvén waves by transfer to protons [see *Hu et al.,* 1997; *Li et al.,* 1997] is 1.67 ergs cm^{-2} s^{-1}. In the transferred energy flux, 1.16 ergs cm^{-2} s^{-1} is lost by heating protons. Hence the Alfvén waves carry all the energy needed to accelerate and heat the solar wind. The acceleration is achieved primarily by heating the protons and to a lesser extent via the wave force. The pressure gradient force of the heated protons accelerates the wind more readily than the wave force.

3.3. Role of the Correlation Length

We consider next the role of the correlation length. As shown by *Hollweg and Johnson* [1988] and *Isenberg* [1990], decreasing the correlation length can lead to more efficient coronal heating. In the example of Figure 2 (model 2), all parameters in (32) are unchanged except for the correlation length, which is reduced to $(L_c/\Gamma)_{1R_s} = 2\times10^4$ km. (This is comparable to the diameter of a supergranule.) As a result of the smaller correlation length, the heating rate (equation (25)) increases at the coronal base and waves deposit more energy in the subsonic region, leading to a slower wind [*Leer and Holzer,* 1980]. The resulting higher density in this model (see Figure 2b) increases the Coulomb collisions between protons, thus leading to stronger energy exchange between the parallel and perpendicular degrees of freedom. Hence $T_{p\perp}$ does not increase as much in the inner corona, and the anisotropy is much smaller than in the previous model. $Q_{p\|}$ and $Q_{p\perp}$ decrease much more rapidly with heliocentric distance, and the radial distances over which $Q_{p\|}<0$ are much larger in model 2 compared to model 1. Consequently, $T_{p\perp}$ and $T_{p\|}$ decrease more significantly at larger distances, leading to a very large anisotropy there. The effect of the spiral field on cooling $T_{p\|}$ is also more pronounced in this model (Figure 2e) due to the fact that a slower wind speed makes the angle Φ larger than in model 1. Compared to model 1, the wave force is even less important than the proton pressure gradient force. $\langle\delta B^2\rangle^{1/2}/B$ is reduced to 0.1 at 1 AU due to the significant damping of the waves.

Figure 2

3.4. Effect of Rapid Divergence

To explore the effect of a faster than radially expanding flux tube, the following choice of parameters is made:

$$\begin{aligned} f_m &= 5,\ r_a = 1.31\ R_s,\ \sigma_a = 0.51\ R_s,\\ (L_c/\Gamma)_{1R_s} &= 3.37\times10^4\ \text{km},\\ Q_{e0} &= 2.5\times10^{-14}\ \text{erg s}^{-1},\ \sigma_e = 0.2\ R_s. \end{aligned} \qquad (35)$$

To achieve a fast wind model at 1 AU similar to model 1, a smaller correlation length had to be adopted. The results of model 3 are shown in Figure 3. In this case, heat addition to electrons was needed to produce a fast wind comparable to model 1. Comparison with model 1 shows that the electrons are cooler, the acceleration is faster in the inner corona, and the anisotropy is larger at 1 AU.

Figure 3

3.5. Dissipation at the Kraichnan Rate With $\eta = 5/3$

We explore next the cascading process proceeding at the Kraichnan rate with $\eta = 5/3$. By comparing equation (25) with (26), it is clear that to achieve heating rates comparable to those used in model 1 for a fast wind, a much smaller correlation length must be chosen in this case, since v_A is large in the inner corona. Hence the following parameters

$$\begin{aligned} (L_c/\Gamma)_{1R_s} &= 8000\ \text{km},\\ Q_{e0} &= 2\times10^{-14}\ \text{erg s}^{-1},\ \sigma_e = 0.2\ R_s, \end{aligned} \qquad (36)$$

are used in the calculations. As in models 1 and 2, radial expansion is again assumed.

Figure 4

Model 4, shown in Figure 4, yields a high-speed wind. In this case, it was necessary to apply additional heating to the electrons to obtain a solar wind solution, since the Kraichnan rate yields less heating to balance the radiation loss for electrons than in model 1. In comparison with model 1, the acceleration of the wind is much more pronounced in the inner corona, and the cooling in the parallel direction is stronger very close to the coronal base, but slightly weaker at large distances. Subsequently, the anisotropy at 1 AU (Figure 4d) is much larger than in model 1 (Figure 1d). The momentum due to the wave force (Figure 4f) decreases much more rapidly beyond 10 R_s than in model 1 (Figure 1f). The quantity $\langle \delta B^2 \rangle^{1/2}/B$ is slightly lower than observed at 1 AU (Figure 4d).

The effects of rapid divergence with the Kraichnan rate are identical to those of the Kolmogorov rate (see section 3.4). For $f_m > 1$, the correlation length needs to be decreased even further since the Alfvén speed will increase more rapidly as the density gradient decreases more sharply.

3.6. Dissipation at the Kolmogorov Rate With $\eta = 3$

In the computations presented so far, we considered a slope of $\eta = 5/3$ for the entire power spectrum. Recent observations by *Leamon et al.* [1998], however, indicate that a much steeper spectrum could be present in the dissipation range. Given in Figure 5 is a comparison between model 1 and the same parameters except for $\eta = 3$ in the dissipation range where equations (22)-(24) apply. The main effect of the steeper slope is to increase the cooling of the protons in the parallel direction beyond 6 R_s (Figure 5a) due to the extended heat loss to the parallel direction when compared to model 1 (Figure 5b).

Figure 5

3.7. Latitudinal Dependence of the Temperature Anisotropy

The empirical values used for comparison of our computations with inferences of temperatures, densities, and wave velocity amplitudes were derived from remote sensing observations in polar regions in the inner corona, and from in situ observations both in the ecliptic plane from Helios, as well as over the poles from Ulysses. Unfortunately, no measurements of the coronal magnetic field are currently available, and no temperature anisotropy measurements were made by Ulysses at high latitude. To fill the gap between the ecliptic and high-latitude observations, we therefore show the latitudinal dependence of the temperature anisotropies for a range of values of the magnetic field strength at 1 AU. The parameters used in these computations are for the Kolmogorov rate of model 1. As shown in Table 1, the strength of the magnetic field at 1 AU, B_{rE}, is varied from 3.5 to 6 γ, and the wave velocity amplitude and correlation length are adjusted in such a way that both $\left(\Gamma \left\langle \delta v^2 \right\rangle^{3/2} / L_c\right)_{1R_s}$ and $B_{rE} \left(\left\langle \delta v^2 \right\rangle\right)_{1R_s}$ are fixed, so that the same heating function and high-speed wind can be achieved (see equation (25) and *Hu et al.* 1997]). The behavior of the anisotropy, $T_{p\parallel}/T_{p\perp}$ at 1 AU, versus latitude is shown in Figure 6. We note that for a field strength of 3.5 γ no solar wind solutions could be found for $\theta < 20°$, since for those values $A < 0$ at 1 AU. In all cases, the anisotropy increased as a function of latitude, as the effect of the spiral field decreased.

Table 1

Figure 6

3.8. Summary

The prime free parameter in the model computations presented above is the correlation length. While it has a physical meaning, namely, the mean flux tube separation, presently there is no empirical measure for this quantity, especially close to the Sun, where the principal heating occurs. Moreover, the heating rate includes the unknown factor Γ, which is presumed to be of order 1, but again, we have no way of calibrating this quantity especially close to the Sun. (However, see *Verma et al.* [1995]). It is clear that the applicability of the proposed mechanism for the two dissipation rates considered depends critically on the value of the correlation length and that the value is different for the two rates.

What these calculations have shown is that the cooling needed for the protons in the direction parallel to the magnetic field, as pointed out originally by *Hu et al.* [1997], is a natural consequence of the mechanism proposed. The waves provide a natural mechanism for the extraction of energy from the parallel direction, hence the cooling of the parallel proton temperature, and feeding that energy into the perpendicular direction. Subsequently, the observed anisotropy in the proton temperature is achieved.

At the same time, these models have shown that a heating rate determined by a turbulent cascade, with dissipation occurring via the cyclotron resonance, is capable of producing high-speed solar wind flows with densities and proton temperatures in the corona and far from the Sun which are consistent with currently available observations.

4. Discussion and Conclusions

This study demonstrates that parallel propagating nondispersive ion cyclotron waves in the fast solar wind can play a significant role in shaping the proton temperature anisotropy in both the inner corona and interplanetary space. An essential feature of the model is the assumption that the ion cyclotron waves are produced by a turbulent cascade from large spatial scales, where most of the power is presumed to be concentrated. Indeed, in situ measurements of power spectra of Alfvénic fluctuations show that most of the power is at large scales [e.g., *Tu and Marsch*, 1990], as do power spectra of magnetic field fluctuations close to the Sun [*Hollweg et al.*, 1982; *Andreev et al.*, 1997]. Another essential assumption of the model is that the turbulent cascade itself determines the overall heating rate. Thus the main role of the ion cyclotron waves is to determine how the dissipated energy is apportioned between the parallel and perpendicular components. In effect, the turbulent cascade determines the level of power at the resonant frequencies, providing closure to the model. Ion cyclotron waves are found to be able to substantially heat the protons in the direction perpendicular to the magnetic field. At the same time the waves can heat or cool protons in the parallel direction in different regions: $T_{p\|}$ is heated in the region where $T_{p\perp}$ is much larger than $T_{p\|}$; this happens from several solar radii to about 50 R_s. At the coronal base and beyond 50 R_s, protons are cooled in the parallel direction, but the parallel cooling at the coronal base is quite small. Our computations show that ion cyclotron waves not only cause a strong proton temperature anisotropy in the inner corona but also limit the growth of proton temperature anisotropy in interplanetary space.

We limited this study to nondispersive waves. However, we have to keep in mind that waves in the solar wind might be dispersive at the high-frequencies where the cyclotron resonance occurs. The heating and cooling effects of the dispersive waves on the wind may be quite different and the waves may constrain the anisotropy development even more. However, this has to be proven. The study also assumed parallel propagating waves in the dissipative range. It is doubtful, however, that the turbulent cascade proceeds only along $k_\|$, and refraction in a structured corona will tend to increase $k_\perp$. Resonant interactions with obliquely propagating waves can be substantially different from those with parallel propagating waves [e.g., *Harmon*, 1989]. For example, both the Alfvén and fast-mode branches of the dispersion relation will be elliptically polarized at high frequencies. Thus protons will be able to resonate with some of the fast-mode power, while the electrons will be heated [e.g., *Habbal and Leer*, 1982], an effect which is not included in the present study. Since the mechanism presented here does not provide any extended heating to electrons, and because of the weak coupling between electrons and protons, our models produce very low electron temperatures in both the inner corona and interplanetary space. Our high-speed models 1, 3, and 4 have a temperature dip at the coronal base, indicating the mechanisms used in the present study do not account for the energy needed to heat the electrons and protons in the region where radiation losses are still significant. Hence our study may suggest that to match observed values, a mechanism to heat electrons is required. Alternatively, given the uncertainty in the transition region observations, where both the temperature and density are varying rapidly with height, the dip may simply indicate that we have chosen a value for the base pressure which is somewhat too high.

We have also neglected the modification of the dispersion relation by He^{++} and other heavy ions. The combined effects of oblique propagation and He^{++} on the resonant interaction remain to be explored. We note too that our use of the WKB approximation to describe the evolution of the low-frequency wave power (equations (15)-(18)) cannot really be justified in view of the very large Alfvén speeds in a low-density coronal hole, which presumably lead to large wavelengths. However, an alternative description is not available. Finally, we note that a WKB description of Alfvénic waves is not consistent with the existence of turbulence. The reason is that turbulence is driven by the generalized Reynolds stress, $\rho\mathbf{v}\cdot\nabla\mathbf{v} - \mathbf{B}\cdot\nabla\mathbf{B}/4\pi$, which vanishes for WKB Alfvénic waves. Thus our use of either the Kolmogorov or Kraichnan heating rates has to be viewed as an Ansatz, which at least leads to models resembling reality. The presence of turbulent power spectra in the corona and in interplanetary space suggests that our Ansatz is reasonable, but does not constitute a proof. (See also *Hollweg* [1984] for some physically motivated arguments about how a Kolmogoroff cascade might develop.)

To be consistent with the observed proton heat flux, we have used a very simple assumption for the proton thermal conduction. It has been shown that the proton and electron heat fluxes can be better described with an eight-moment description [*Olsen and Leer,* 1996]. For the solar wind with anisotropic protons, a higher moment description of the proton heat flux will be needed.

We find that both the Kolmogorov and Kraichnan energy cascading functions can be used to describe the heating and acceleration of protons in a manner generally consistent with the observed behavior of high-speed streams. With the use of the Kraichnan rate, a much smaller correlation length must be used to damp the Alfvén waves. When a faster than radial expansion of the field lines is taken into account, the correlation length for both mechanisms has to be decreased compared to radial expansion. Existing observations are not capable of distinguishing between the two processes.

Appendix

In this appendix, we derive the expression for the Alfvén wave force in a two-fluid plasma with anisotropic protons. Neglecting the rotation of the Sun, the wave force F_w on the protons can be written as [*Isenberg*, 1984]

$$F_w = \rho_p \frac{d}{dr}\left[\frac{4\pi p_w}{B^2}(\omega^2/k_\parallel^2 - v^2)\right] + \frac{Q_p}{\omega/k_\parallel - v}. \quad \text{(A1)}$$

In a time-independent system, the wave action equation in a two-fluid plasma is

$$\nabla\cdot(\omega \mathbf{S}) = -Q_p \frac{\omega}{k_\parallel}\left(\frac{\omega}{k_\parallel} - v\right)^{-1}, \quad \text{(A2)}$$

where

$$\omega \mathbf{S} = \frac{\langle \delta B^2\rangle}{4\pi v_A^2}\left(\frac{\omega}{k_\parallel}\right)^2\left(\frac{\omega}{k_\parallel} - v\right)\mathbf{B}/B. \quad \text{(A3)}$$

So we have

$$F_w/\rho_p = \frac{d}{dr}\left[\frac{\langle \delta B^2\rangle}{2B^2}\left(v_A^2 A + 2 v v_A A^{1/2}\right)\right] -$$

$$\frac{1}{\rho_p \frac{\omega}{k_\parallel}}\frac{1}{a}\frac{d}{dr}\left[\frac{a\langle \delta B^2\rangle}{4\pi v_A^2}\frac{\omega^2}{k_\parallel^2}\left(\frac{\omega}{k_\parallel} - v\right)\right]$$

$$= \frac{d}{dr}\left[\frac{\langle \delta B^2\rangle}{2B^2}\left(v_A^2 A + 2 v v_A A^{1/2}\right)\right]$$

$$-\frac{1}{\rho_p \frac{\omega}{k_\parallel}}\frac{1}{a}\frac{d}{dr}\left[\frac{a\langle \delta B^2\rangle}{4\pi v_A^2}\frac{\omega}{k_\parallel}\left(v v_A A^{1/2} + v_A^2 A\right)\right]. \quad \text{(A4)}$$

In the last term on the right-hand side of (A4), we have

$$\frac{d}{dr}\left[\frac{a\langle \delta B^2\rangle}{4\pi v_A^2}\frac{\omega}{k_\parallel}v_A^2 A\right] = \frac{d}{4\pi dr}\left[\langle \delta B^2\rangle A^2 \frac{a}{A}\frac{\omega}{k_\parallel}\right]$$

$$= \frac{1}{4\pi}\frac{a}{A}\frac{\omega}{k_\parallel}\frac{d}{dr}\left(\langle \delta B^2\rangle A^2\right) + \frac{\langle \delta B^2\rangle A^2}{4\pi}\frac{d}{dr}\left(\frac{a}{A}\frac{\omega}{k_\parallel}\right). \quad \text{(A5)}$$

Thus, (A4) can be written as

$$F_w/\rho_p = \frac{d}{dr}\left[\frac{\langle \delta B^2\rangle}{B^2} v v_A A^{1/2}\right] - \frac{\langle \delta B^2\rangle A^2}{\rho_p \frac{\omega}{k_\parallel} a 4\pi}\frac{d}{dr}\left[\frac{a}{A}\frac{\omega}{k_\parallel}\right]$$

$$-\frac{1}{4\pi\rho_p \frac{\omega}{k_\parallel} a}\frac{d}{dr}\left[\frac{a\langle \delta B^2\rangle}{v_A}\frac{\omega}{k_\parallel} v A^{1/2}\right] + \frac{\langle \delta B^2\rangle A^2}{8\pi}\frac{d}{dr}\left(\frac{1}{\rho_p A}\right)$$

$$-\frac{1}{8\pi\rho_p A}\frac{d}{dr}(\langle \delta B^2\rangle A^2) \quad \text{(A6)}$$

and the third term on the right-hand side of (A6) is

$$-\frac{1}{4\pi\rho_p \frac{\omega}{k_\parallel} a}\frac{d}{dr}\left[\left(\frac{a}{A}\frac{\omega}{k_\parallel}\right)\times\left(\frac{\langle \delta B^2\rangle}{v_A} v A^{3/2}\right)\right] =$$

$$-\frac{\frac{a}{A}\frac{\omega}{k_\parallel}}{4\pi\rho_p a \frac{\omega}{k_\parallel}}\frac{d}{dr}\left[\frac{\langle \delta B^2\rangle}{v_A} v A^{3/2}\right] - \frac{\langle \delta B^2\rangle v A^{3/2}}{4\pi\rho_p a \frac{\omega}{k_\parallel} v_A}\frac{d}{dr}\left[\frac{a}{A}\frac{\omega}{k_\parallel}\right]$$

$$= -\frac{1}{4\pi\rho_p A}\frac{d}{dr}\left[\frac{\langle \delta B^2\rangle}{v_A} v A^{3/2}\right]$$

$$-\frac{\langle \delta B^2\rangle A^{3/2} v}{4\pi\rho_p a v_A (v + v_A A^{1/2})}\frac{d}{dr}\left[\frac{a}{A}\frac{\omega}{k_\parallel}\right].$$

We then have for (A6)

$$F_w/\rho_p = \frac{d}{dr}\left[\frac{\langle \delta B^2\rangle A^{1/2}}{4\pi\rho_p v_A} v\right] - \frac{A^{3/2}\langle \delta B^2\rangle}{4\pi\rho_p a v_A}\frac{d}{dr}\left[\frac{a}{A}\frac{\omega}{k_\parallel}\right]$$

$$-\frac{1}{4\pi\rho_p A}\frac{d}{dr}\left[\frac{\langle \delta B^2\rangle}{v_A} v A^{3/2}\right] - \frac{\langle \delta B^2\rangle}{8\pi\rho_p^2}\frac{d(\rho_p A)}{dr}$$

$$-\frac{1}{8\pi\rho_p A}\frac{d}{dr}(\langle \delta B^2\rangle A^2)$$

$$= -\frac{\langle \delta B^2\rangle v}{4\pi\rho_p^2 A^{1/2} v_A}\frac{d}{dr}(\rho_p A) - \frac{A^{3/2}\langle \delta B^2\rangle}{4\pi\rho_p a v_A}\frac{d}{dr}\left(\frac{a}{A}\frac{\omega}{k_\parallel}\right)$$

$$-\frac{\langle \delta B^2\rangle}{8\pi\rho_p^2}\frac{d}{dr}(\rho_p A) - \frac{1}{8\pi\rho_p A}\frac{d}{dr}(\langle \delta B^2\rangle A^2). \quad \text{(A7)}$$

We notice that

$$\frac{a}{A}\frac{\omega}{k_\parallel} = \frac{\rho_p a v}{\rho_p A} + \frac{aB}{\sqrt{4\pi\rho_p A}}$$

so the first three terms of (A7) add up to zero, and F_w can be written in the very compact form of

$$F_w = -\frac{1}{8\pi A}\frac{d}{dr}(\langle \delta B^2\rangle A^2). \quad \text{(A8)}$$

Equation (A8) is identical to the result given by *Barnes* [1979] for the case of zero dissipation. We see now that (A8) holds even when dissipation is included.

When the spiral magnetic field is considered, the above equations are still valid in the corotating frame, since the magnetic field is parallel to the flow speed. Hence (A8) is still valid in that case.

Acknowledgments. This work was supported by NASA grants NAG5-6271, NAG5-6215, and NAG5-7055 to the Smithsonian Astrophysical Observatory. Partial support for X. Li was also provided by a predoctoral fellowship from the Smithsonian Astrophysical Observatory. J.V. Hollweg was supported by the NASA Space Physics Theory Program under grant NAG5-1479 to the University of New Hampshire.

The Editor thanks William Coles and another referee for their assistance in evaluating this paper.

References

Allen, L.A., S.R. Habbal, and Y.-Q. Hu, Thermal coupling of protons and neutral hydrogen in the fast solar wind, *J. Geophys. Res., 103*, 6551, 1998.

Andreev, V.E., A.I. Efimov, L.N. Samoznaev, I.V. Chashei, and M.K. Bird, Characteristics of coronal Alfvén waves deduced from helios Faraday rotation measurements, *Sol. Phys., 176*, 387, 1997.

Arunasalam, V., Quasilinear theory of ion-cyclotron-resonance heating of plasmas and associated longitudinal cooling, *Phys. Rev. Lett., 37,* 746, 1976.

Axford, W.I., and J.F. McKenzie, Acceleration of the solar wind, in *Solar Wind 8*, edited by D. Winterhalter, J.T. Gosling, S.R. Habbal, W.S. Kurth, and M. Neugebauer, p. 72, AIP CP 385, New York, 1995.

Balogh, A., R.J. Forsyth, T.S. Horbury, and E.J. Smith, Variances and fluctuations if the heliospheric magnetic field in solar polar flows, in *Solar Wind 8*, edited by D. Winterhalter, J.T. Gosling, S.R. Habbal, W.S. Kurth, and M. Neugebauer, p. 221, AIP CP 385, New York, 1995.

Barnes, A., Hydromagnetic waves and turbulence in the solar wind, in *Solar System Plasma Physics*, edited by E.N. Parker, C.F. Kennel, and L.J. Lanzerotti, pp. 249-319, North-Holland, New York, 1979.

Barnes, A., and G.C.J. Suffolk, Relative kinetic theory of the large-amplitude transverse Alfvén waves, *J. Plasma Phys., 5,* 315, 1971.

Bavassano, B., M. Dobrowolny, F. Mariani, and N.F. Ness, Radial evolution of power spectra of interplanetary Alfvénic turbulence, *J. Geophys. Res., 87,* 3617, 1982.

Behannon, K.W., Heliocentric distance dependence of the interplanetary magnetic field, *Rev. Geophys., 16*, 125, 1978.

Belcher, J.W., and L. Davis Jr., Large-amplitude Alfvén waves in the interplanetary medium, *J. Geophys. Res., 76,* 3534, 1971.

Braginskii, S. I., Transport phenomena in a plasma, in *Reviews of Plasma Physics*, vol.1, p. 205, Consult. Bur., New York, 1965.

Busnardo-Neto, J., J. Dawson, T. Kamimura, and A.T. Lin, Ion-cyclotron resonance heating of plasmas and associated longitudinal cooling, *Phys. Rev. Lett., 36*, 28, 1976.

Dulk, G. A., K. V. Sheridan, S. F. Smerd, and G. L. Withbroe, Radio and EUV observations of a coronal hole, *Sol. Phys., 52,* 349, 1977.

Dusenbery, P.B., and J.V. Hollweg, Ion-cyclotron heating and acceleration of solar wind minor ions, *J. Geophys. Res., 86,* 152, 1981.

Esser, R., T.E. Holzer, and E. Leer, Drawing inferences about solar wind acceleration from coronal minor ion observations, *J. Geophys. Res., 92*, 13377, 1987.

Esser, R., S.R. Habbal, W.A. Coles, and J.V. Hollweg, Hot protons in the inner corona and their effects on the flow properties of the solar wind, *J. Geophys. Res., 102,* 7063, 1997.

Esser, R., R.J. Edgar, and N.S. Brickhouse, High minor ion outflow speeds in the inner corona and observed ion charge states in interplanetary space, *Astrophys. J., 398*, 448, 1998a.

Esser, R., S. Fineschi, D. Dobrzycka, S.R. Habbal, R.J. Edgar, J.C. Raymond, J.L. Kohl, Plasma properties in coronal holes derived from measurements of minor ion spectral lines and polarized white light intensity, *Astrophys. J. Lett.*, in press, 1998b.

Fisher, R.R., and M. Guhathakurta, Physical properties of the polar coronal rays and holes as observed with SPARTAN 201-01 coronagraph, *Astrophys. J., 447*, L139, 1995.

Habbal, S.R., and E. Leer, Electron heating by fast mode magnetohydrodynamic waves in the solar wind emanating from coronal holes, *Astrophys. J., 253*, 318, 1982.

Habbal, S.R., R. Esser, and M.B. Arndt, How reliable are coronal hole temperatures deduced from observations? *Astrophys. J., 413*, 435, 1993.

Harmon, J.K., Compressibility and cyclotron damping in the oblique Alfvén wave, *J. Geophys. Res., 94*, 15,399, 1989.

Hollweg, J. V., Resonances of coronal loops, *Astrophys. J., 277*, 392, 1984.

Hollweg, J.V., Transition region, corona, and solar wind in coronal holes, *J. Geophys. Res., 91*, 4111, 1986.

Hollweg, J.V., and W. Johnson, Transition region, corona, and solar wind in coronal holes: some two-fluid models, *J. Geophys. Res., 93,* 9547, 1988.

Hollweg, J.V., M.K. Bird, H. Volland, P. Edenhofer, C.T. Stelzried, and B.L. Seidel, Possible evidence for coronal Alfvén waves, *J. Geophys. Res., 87,* 1, 1982.

Hu, Y.Q., R. Esser, and S.R. Habbal, A fast solar wind model with anisotropic proton temperature, *J. Geophys. Res., 102,* 14661, 1997.

Isenberg, P.A., Resonant acceleration and heating of solar wind ions: Anisotropy and dispersion, *J. Geophys. Res., 89,* 6613, 1984.

Isenberg, P.A., Investigations of a turbulence-driven solar wind model, *J. Geophys. Res., 95,* 6437, 1990.

Isenberg, P.A., and J.V. Hollweg, Finite amplitude Alfvén waves in a multi-ion plasma: propagation, acceleration and heating, *J. Geophys. Res., 87,* 5023, 1982.

Isenberg, P.A., and J.V. Hollweg, On the preferential acceleration and heating of the solar wind heavy ions, *J.*

Geophys. Res., 88, 3923, 1983.
Kohl, J.L., et al., The ultravilolet coronagraph spectrometer for the Solar and Heliospheric Observatory, *Sol. Phys., 162*, 313, 1995.
Kohl, J.L., L. Strachan, and L.D. Gardner, Measurement of hydrogen velocity distributions in the extended solar corona, *Astrophys. J., 465,* L141, 1996.
Kohl, J.L., et al., UVCS/SOHO empirical determinations of anisotropic velocity distributions in the solar corona, *Astrophys. J., 501*, L127, 1998.
Kopp, R.A., and T.E. Holzer, Dynamics of coronal hole regions, 1, Steady polytropic flow with multiple critical points, *Sol. Phys., 49*, 43, 1976.
Leamon, R.J., C.W. Smith, N.F. Ness, W.H. Matthaeus, and H.K. Wong, Observational constraints on the dynamics of the interplanetary magnetic field dissipation range, *J. Geophys. Res., 103*, 4775, 1998.
Leer, E., and W.I. Axford, A two-fluid solar wind model with anisotropic proton temperature, *Sol. Phys., 23,* 238, 1972.
Leer, E., and T.E. Holzer, Energy addition in the solar wind, *J. Geophys. Res., 85*, 4681, 1980.
Li, X., R. Esser, S.R. Habbal, and Y.Q. Hu, Influence of heavy ions on the high speed solar wind, *J. Geophys. Res., 102,* 17419, 1997.
Li, X., S.R. Habbal, J.L. Kohl, and G.C. Noci, The effect of temperature anisotropy on observations of Doppler dimming and pumping in the inner corona, *Astrophys. J., 501*, L133, 1998.
Marsch, E., K.-H. Mühlhäuser, R. Schwenn, H. Rosenbauer, W. Pilipp, and F.M. Neubauer, Solar wind protons: Three dimensional velocity distributions and derived plasma parameters measured between 0.3 AU and 1 AU, *J. Geophys. Res., 87,* 52, 1982a.
Marsch, E., C.K. Goertz, and K. Richter, Wave heating and acceleration of solar wind ions by cyclotron resonance, *J. Geophys. Res., 87,* 5030, 1982b.
Marsch, E., W.G. Philip, K.M. Thieme, and H. Rosenbauer, Cooling of solar wind electrons inside 0.3 AU, *J. Geophys. Res. 94*, 6893, 1989.
McKenzie, J. F., M. Banaszkiewicz, and W.I. Axford, Acceleration of the high speed solar wind, *Astron. Astrophys., 303*, L45, 1995.
McKenzie, J. F., M., Banaszkiewicz, and W.I. Axford, The fast solar wind, *Geophys. Res. Lett., 24*, 2877, 1997.
Olsen, E.L., and E. Leer, An eight-moment approximation two-fluid model of the solar wind, *J. Geophys. Res., 101,* 15591, 1996.
Roberts, D.A., Interplanetary observational constraints on Alfvén waves acceleration of the solar wind, *J. Geophys. Res., 94*, 6899, 1989.
Rosner, R., W.H. Tucker, and G.S. Vaiana, Dynamics of the quiescent solar corona, *Astrophys. J., 220*, 643, 1978.
Sandbæk, Ø., and E. Leer, Acceleration and heating of two-fluid solar wind by Alfvén waves, *Astrophys. J., 423,* 500, 1994.
Schwenn, R., Large-scale structures of the interplanetary medium, in *Physics of the Inner Heliosphere I, Large Scale Phenomena*, edited by R. Schwenn and E. Marsch, p. 99, Springer-Verlag, New York, 1990.
Smith, E.J., A. Balogh, M. Neugebauer, and D. McComas, Ulysses observations of Alfvén waves in the southern and northern solar hemisphere, *Geophys. Res. Lett., 22,* 3381, 1995.
Spitzer, L., Jr., *Physics of Fully Ionized Gases*, Interscience, New York, 1962.
Tu, C.-Y., and E. Marsch, Evidence for a "background" spectrum of solar wind turbulence in the inner heliosphere, *J. Geophys. Res., 95*, 4337, 1990.
Tu, C.-Y., and E. Marsch, MHD structures, waves and turbulence in the solar wind: Observations and theories, *Space Sci. Rev., 73,* 1, 1995.
Tu, C.-Y., and E. Marsch, Two-fluid model for heating of the solar corona and acceleration of the solar wind by high-frequency Alfvén waves, *Sol. Phys., 171,* 363, 1997.
Verma, M.K., D.A. Roberts, and M.L. Goldstein, Turbulent heating and temperature evolution in the solar wind plasma, *J. Geophys. Res., 100*, 19839, 1995.
Villante, U. and M. Vellante, The radial evolution of the IMF fluctuations: A comparison with theoretical models, *Sol. Phys., 81*, 367, 1982.
Withbroe, G.L., Models for the solar transition layer, in *Proceedings of the November 7-10, 1977, OSO-8 Workshop*, p.2, Lab. for Atmos. and Space Phys., Univ. of Color., Boulder, 1977.
Withbroe, G.L., The temperature structure, mass, and energy flow in the corona and inner solar wind, *Astrophys. J., 325,* 442, 1988.

R. Esser, S.R. Habbal, and X. Li, Harvard-Smithsonain Center for Astrophysics, 60 Garden Street, Cambridge, MA 02138. (email: resser@cfa.harvard.edu; shabbal@cfa.harvard.edu; xli@cfa.harvard.edu.)

J.V. Hollweg, Institute for the Study of Earth, Oceans and Space and Department of Physics, University of New Hampshere, Durham, NH 03824. (email: joe.hollweg@unh.edu)

July 23, 1998; revised November 13, 1998; accepted November 13, 1998.

This preprint was prepared with AGU's LaTeX macros v4. File revise formatted September 15, 1999.

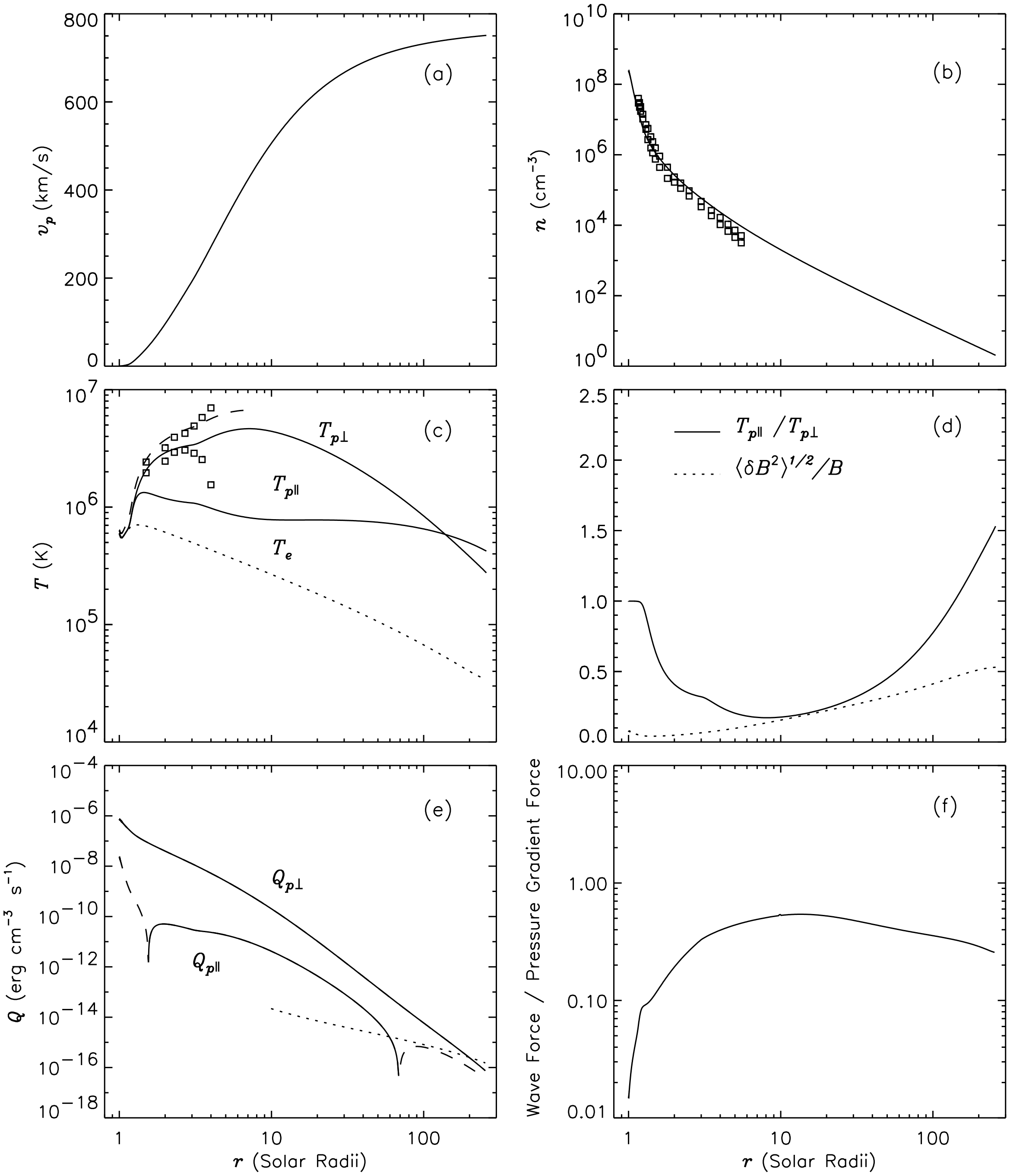

Figure 1. Model 1: a two-fluid solar wind model with anisotropic proton temperature. The model assumes the Kolmogorov heating rate for the protons and radial geometry, with $(L_c/\Gamma)_{1R_s} = 9 \times 10^4$ km: (a) velocity; (b) electron density (the open boxes represent the observed upper and lower electron density limits given by *Fisher and Guhathakurta* [1995]); (c) proton and electron temperatures (the open boxes represent the observed upper and lower perpendicular temperatures of neutral hydrogen derived from the line-width measurements of H I Lyα in coronal holes [*Kohl et al.*, 1998]; (d) temperature anisotropy $T_{p\|}/T_{p\perp}$ (solid line) and Alfvén wave relative amplitude $\langle\delta B^2\rangle^{1/2}/B$ (dotted line); (e) parallel and perpendicular heating rates of protons used in the model (solid and dashed lines correspond to positive and negative values, respectively); and (f) ratio between Alfvén wave force and the pressure gradient force of protons.

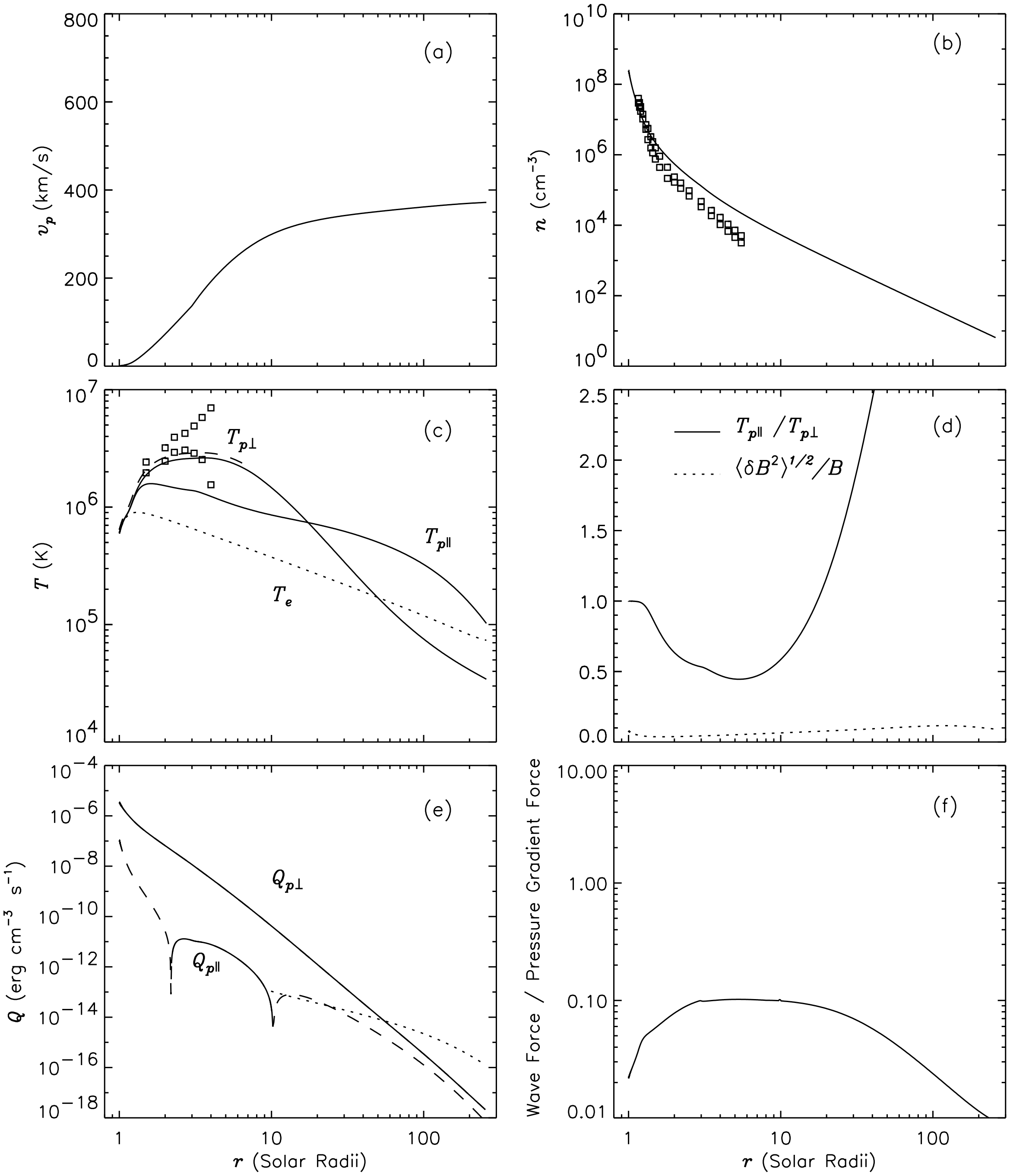

Figure 2. Model 2: same as Figure 1 for $(L_c/\Gamma)_{1R_s} = 2\times10^4$ km.

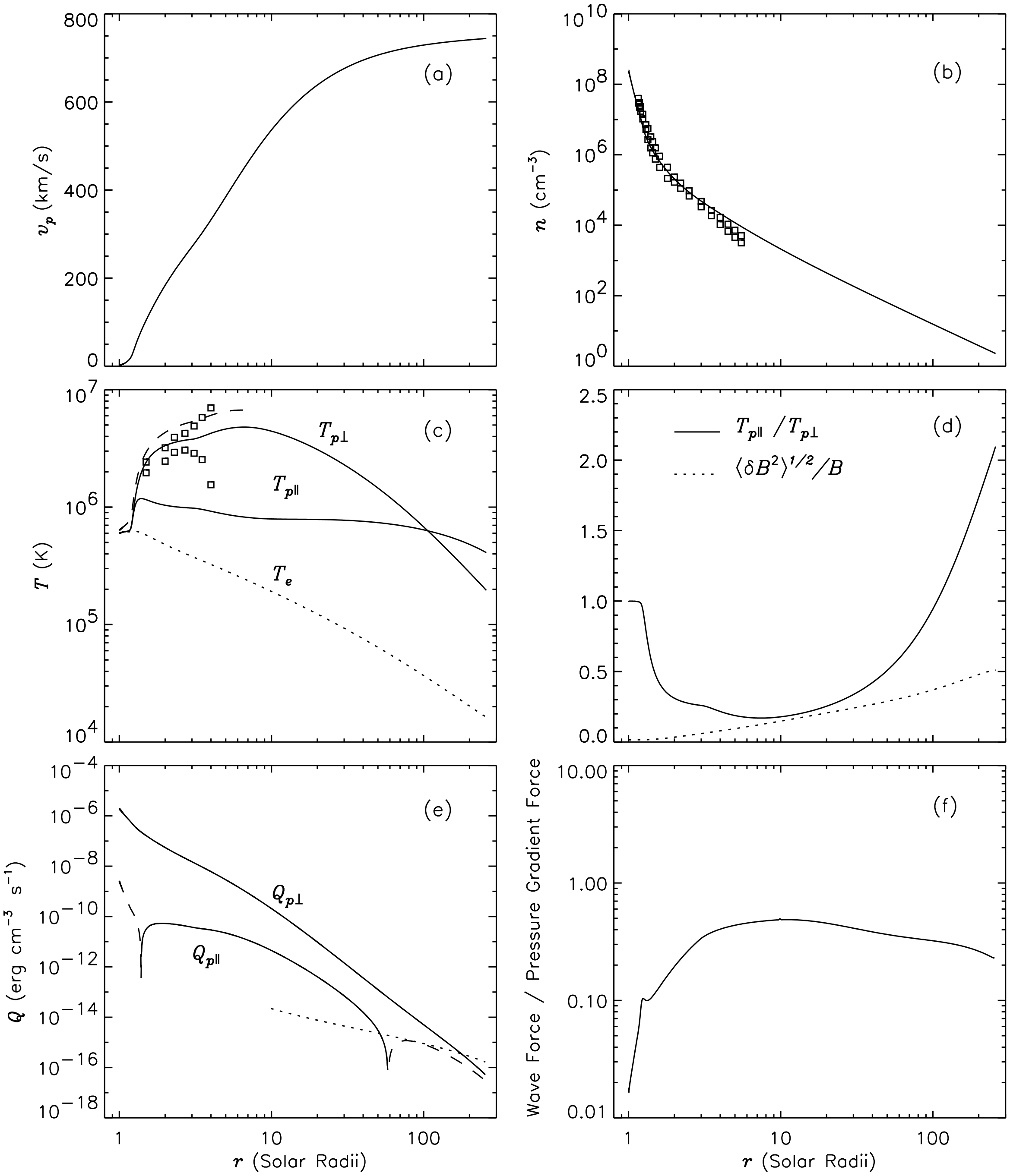

Figure 3. Model 3: same as Figure 1 for $f_m = 5$, and $(L_c/\Gamma)_{1R_s} = 3.4 \times 10^4$ km.

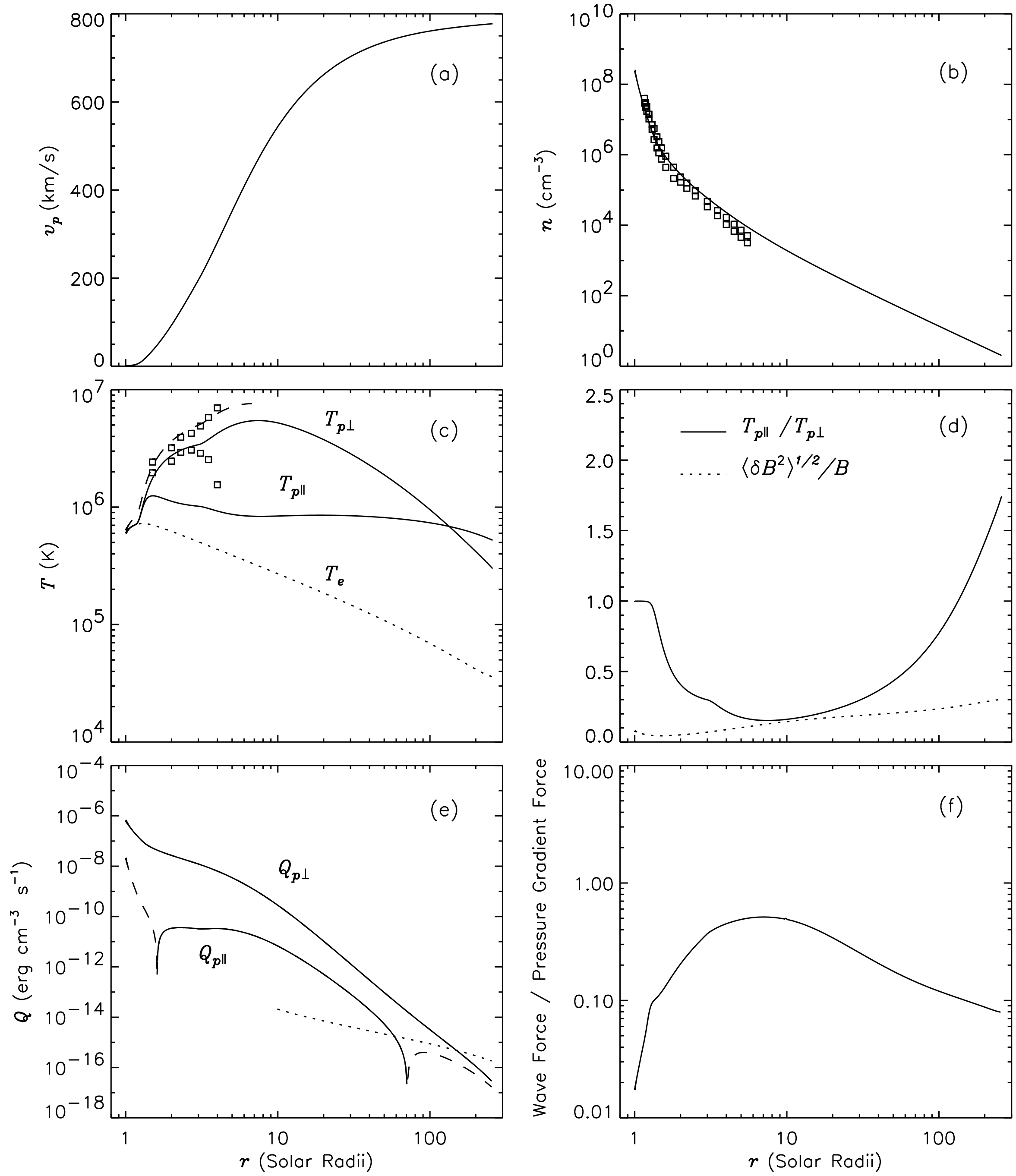

Figure 4. Model 4: same as Figure 1 for the Kraichnan dissipation rate and $(L_c/\Gamma)_{1R_s} = 8000$ km.

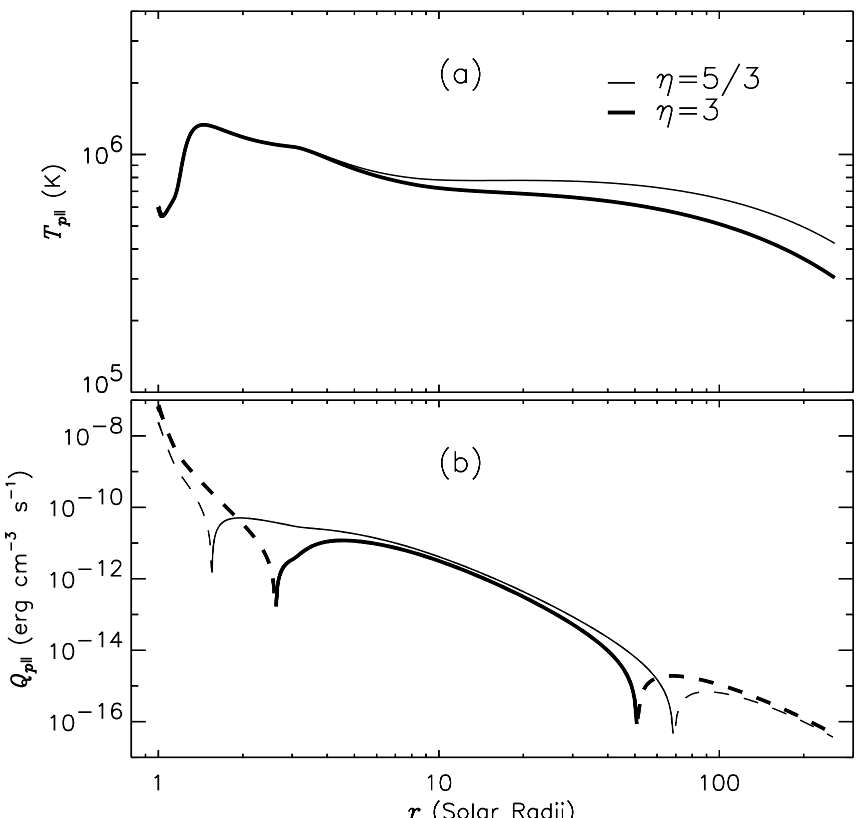

Figure 5. Comparison of temperatures and heating rates for a spectral index of $\eta = 5/3$ (thin line) and 3 (thick line) for the Kolmogorov dissipation rate. The other parameters are the same as for model 1.

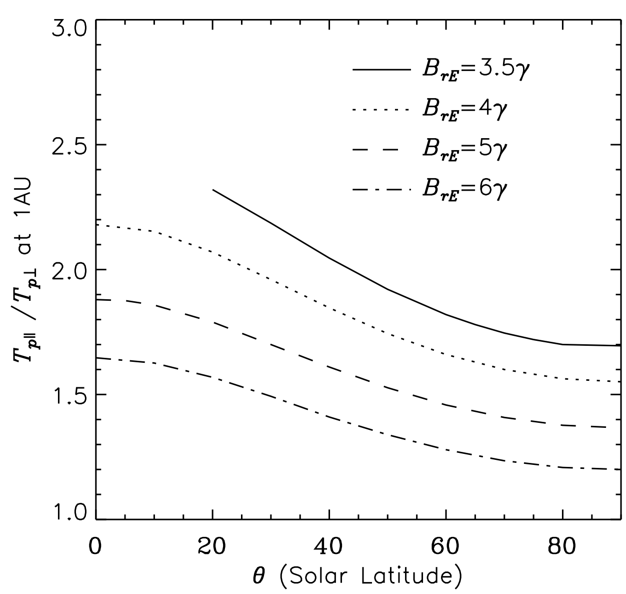

Figure 6. Latitudinal dependence of the temperature anisotropy at 1 AU for a range of magnetic field values, B_{rE}, at 1 AU.

Table 1. Parameters Used for the latitudinal dependence of the temperature anisotropy

B_{rE}	$\left(\langle\delta v^2\rangle^{1/2}\right)_{1R_s}$, km/s	$(L_c/\Gamma)_{1R_s}$, km/s	$n_E v_E$, cm^{-2} s^{-1}	v_E, km/s
3.5γ	29.5	1.4×10^5	2.2×10^8	738
4γ	28	1.2×10^5	2.2×10^8	747
5γ	25	9.0×10^4	2.2×10^8	748
6γ	23	7.2×10^4	2.2×10^8	750